Bulletin of the Geological Society of Malaysia, Volume 74, November 2022, pp. 1 - 15
DOI: https://doi.org/10.7186/bgsm74202201

Gas hydrate resource potential of deepwater Sabah, Malaysia: A preliminary assessment

Mazlan Madon

Malaysian Continental Shelf Project, National Security Council, c/o 11th Floor, Wisma JUPEM, Jalan Semarak, 50578 Kuala Lumpur, Malaysia
Author email address: mazlan.madon@gmail.com

Abstract: Offshore NW Sabah is one of the localities identified in the United States Geological Survey (USGS) global hydrates database but not much work has been done on this potential source of energy for Malaysia and the surrounding region. The presence of gas hydrates in this area is mainly inferred from bottom-simulating reflectors (BSR) identified in seismic reflection profiles across the margin. BSRs have been mapped across almost the entire length of the deepwater fold-thrust belt in the Sabah Trough where they are commonly observed within the crests of fold-thrust anticlines. Based on an average geothermal gradient of 62.5 °C/km, the thickness of the gas hydrate stability zone is predicted to vary with water depth from zero at 640 m water depth to 300 m at 2900 m water depth. The total in-place methane resource from the Sabah gas hydrates is estimated to range from 72 to 852 trillion cu. ft. (TCF) (2.06 – 24.1 x 10^{12} m^3) with a mean of 364 TCF (10.3 x 10^{12} m^3) and a most likely (P50) value of 252 TCF (7.1 x 10^{12} m^3). These preliminary estimates may seem large but they are comparable with those from other gas hydrate deposits in the region. More work is required to refine them in order to determine how much of the *in situ* volume is technically and economically recoverable.

Keywords: Offshore Sabah, gas hydrates, bottom-simulating reflector, methane, gas hydrate stability zone, gas resource

INTRODUCTION

Gas hydrate is natural gas, typically methane, trapped in the crystal lattice of ice or water molecules at low temperature and high-pressure subsurface conditions. Due to its restricted stability field, 98% of gas hydrate occur along outer continental margins, beneath the seabed at extreme water depths greater than 500 m in the mid-latitude regions. The remaining 2% occur in permafrost regions where ground temperatures are often below freezing point all year round (Krey *et al.*, 2009; Birchwood *et al.*, 2010; Ruppel, 2018). In permafrost regions, however, gas hydrate deposits tend to be 1.3 to 4.5 times thicker than those in marine settings due to lower temperatures and low geothermal gradients (Wang & Lau, 2020). Methane in gas hydrates is a volumetrically significant potential resource because a unit volume of gas hydrate at reservoir conditions is equivalent to 164 times the volume of methane gas at standard temperature and pressure conditions (Ruppel, 2011).

Gas hydrate deposits, though not yet commercially exploited, have the potential as a significant resource for hydrocarbons in the deep sea and have been touted as the "energy of the future" (Lu, 2015; Ruppel, 2018). As conventional oil and gas reservoirs are gradually depleting from the shallow waters of the continental shelf, more exploration and exploitation activities are being carried out in deep waters. Besides their resource potential, the presence of gas hydrates at continental margins are considered as potential marine geohazards (e.g., Kvenvolden, 1999; Maslin *et al.*, 2010). The presence of gas hydrates may pose a risk to oil and gas infrastructure through seabed instability or through mass wasting processes such as submarine landslides. In addition, natural disruption of large gas hydrate deposits in the seabed, especially the shallow ones, may be triggered by various mechanisms such as seismic activity. This may result in the release of large volumes of methane to the atmosphere and may have adverse impact on climate change (Reagan & Moridis, 2007; Maslin *et al.*, 2010). Thus, it is important to identify and assess the occurrences of gas hydrate deposits, not only for economic purposes, but for potential geohazard and climate change mitigation.

Figure 1 shows the global occurrences of gas hydrates based on the data compiled by Waite *et al.* (2020). Due to its importance, research on gas hydrates is being actively carried out by several countries, including China, United States, Republic of Korea, Japan, Canada, India and Taiwan (Mienert *et al.*, 2022). Major gas hydrate deposits are being studied in the polar regions of Alaska, Norway and Russia. In mid-latitude regions, such deposits include those in the North Atlantic and Gulf of Mexico as well as Central America. In Asia, research activities are being carried out by China, South Korea and Japan. There are several examples of hydrate deposits in the South China Sea region, mostly on its northern margin (Wang *et al.*, 2006; Zhang *et al.*, 2021; Su *et al*., 2022; Wang *et al*., 2022). However, more occurrences are now being reported from the southern and western margins of the South China (Figure 2).

0126-6187; 2637-109X / Published by the Geological Society of Malaysia.

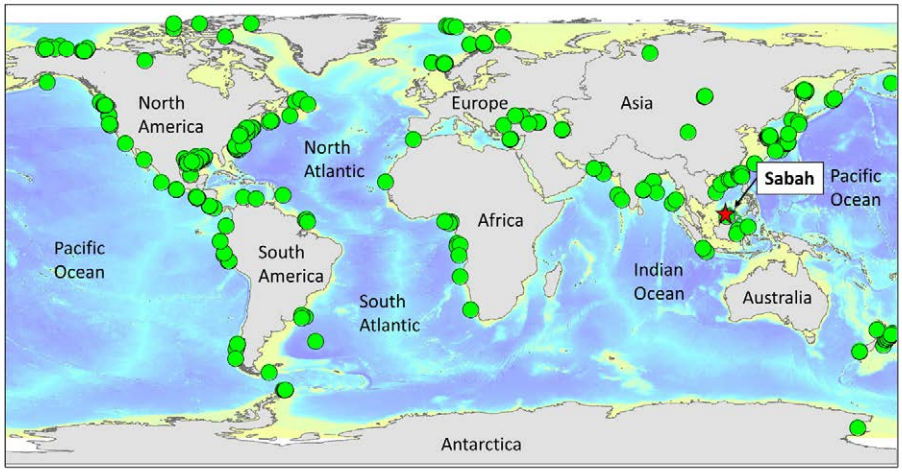

Figure 1: Global distribution of known gas hydrate occurrences based on data downloaded from US Geological Survey (Waite *et al.*, 2020). Sabah is identified as one locality via the Gumusut-Kakap oil field.

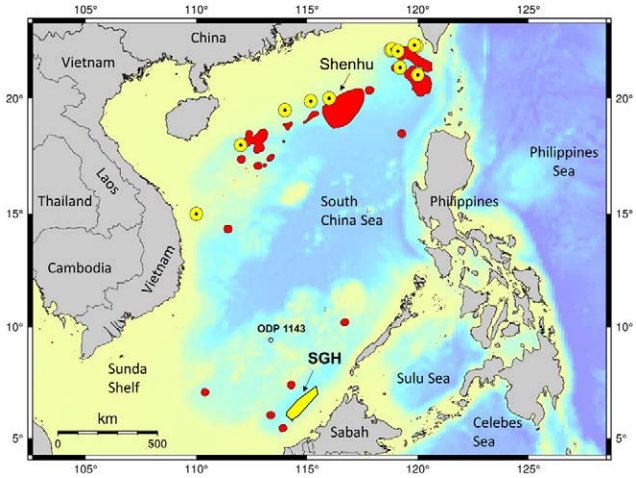

Figure 2: Gas hydrate occurrences in the South China Sea region. Yellow circles with dots are from the USGS database (cf. Figure 1) whereas the red areas and circles are known occurrences based on Wang *et al.* (2006). The Sabah gas hydrates (SGH) is the subject of this study. Also indicated is the Shenhu hydrate area on the northern margin of the South China Sea. ODP site 1143 provided the porosity data shown in Figure 11. The base map is bathymetry from Global Multi-Resolution Topography (GMRT) database (Ryan *et al.*, 2009).

In the deep waters of Sabah, offshore NW Borneo (Malaysia), oil and gas have been discovered in middle Miocene to lower Pliocene turbidite fan units within anticlinal structures that formed on the inner slope of the Sabah Trough (Ingram *et al.*, 2004; Grant, 2005). Since the discovery of the first deepwater oil field at Kikeh in 2002, more than 150 wildcat wells have been drilled in deepwater Sabah. About 80% (over 100) of those have encountered hydrocarbons, mostly in the deepwater fold-thrust belt (DWFTB) (Figure 3). According to Westwood Energy, (2019[1]), 153 exploration wells have been drilled in the region since 2008, resulting in 37 commercial discoveries that have delivered a cumulative recoverable resource of 3.5 billion barrels of oil equivalent (boe), 94% of which is gas. Hence, offshore NW Sabah is proven to be a prolific petroleum province with significant potential for conventional oil and gas production. However, besides the conventional hydrocarbons, it is worthwhile to also explore the potential of unconventional hydrocarbons, since regulatory and development infrastructures are already available.

The presence of gas hydrates offshore Sabah has long been inferred from bottom-simulating reflectors (BSR) identified in seismic reflection profiles across the margin (Hinz *et al.*, 1989). However, not much has been done to map their distribution and estimate the gas resource potential for the future. According to the Malaysia's Petroleum Development Act 1974, ownership of all the hydrocarbon resources in the country including gas hydrates is vested in PETRONAS, the national oil company. Although some studies have been conducted in the past by PETRONAS, the results were never published and information is hardly available in the public domain. A recent review by Nurfadhila *et al.* (2018) reported that gas hydrates in NW Sabah occur in water depths from 1150 to 2700 m, based on the presence of BSRs observed between 250 and 350 m below the seafloor. The gas resource from the Sabah hydrates was estimated to be 173 trillion cu.ft. (TCF) (Nurfadhila *et al.*, 2018). More recently, Goh *et al.* (2017) and Jong *et al.* (2020) described gas hydrates encountered in the Bestari field in the then JX Nippon exploration Block R at the southwestern end of the Sabah Trough. The objective of this paper is to review the available public domain information

[1] Westwood Energy, 2019. "Sabah & Sarawak Basins: Looking deep into NW Borneo"

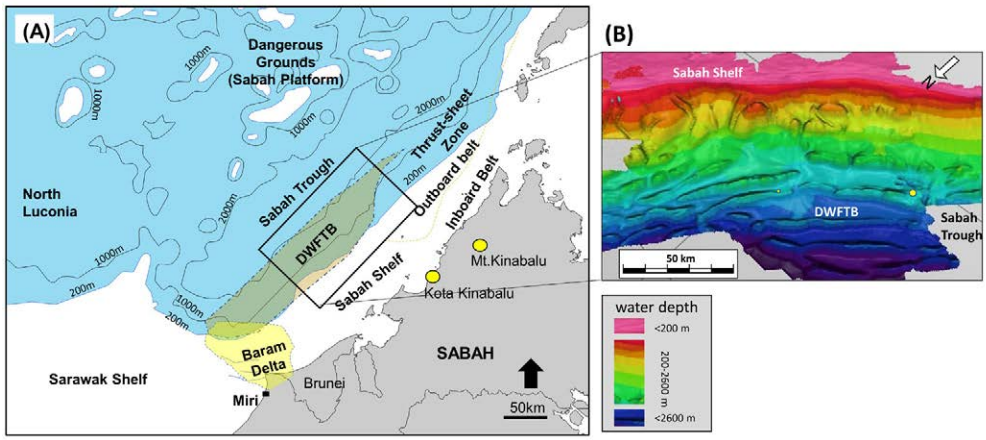

Figure 3: Geological setting of the deepwater fold-thrust belt (DWFTB), offshore Sabah. (A) Bathymetric chart of the region around the DWFTB, which spans the landward side of the Sabah Trough from Baram Delta to the Thrust Sheet Zone. Other elements include the Outboard and Inboard belts (Hazebroek & Tan, 1993). Selected isobaths are shown: 200 m, 1000 m, 2000 m for reference. The rectangular outline is the area shown in B. (B) 3D rendering of the bathymetry of the DWFTB based on seismic-derived bathymetry data, showing the elongated anticlinal ridges subcropping at the seabed which are also targets for exploration drilling. From Madon *et al.* (2015).

on the occurrence and distribution of gas hydrates in the deepwater areas of Malaysia, particularly offshore Sabah. With the available data, an attempt was made to estimate the volume of natural gas resource that may potentially be available to be exploited in the future.

GEOLOGY AND TECTONIC SETTING

The Sabah continental margin comprises a narrow shelf about 80 km wide, flanking a broad region seaward called the Dangerous Grounds (or Sabah Platform) which is underlain by extended continental crust that forms the southern margin of the South China Sea basin (Figure 3A). Between the shelf and platform area is a NE-SW trending, ~85 km wide, 500 km long and 2.9 km deep bathymetric depression known as the Sabah (or NW Borneo) Trough. This feature is generally regarded as a foreland basin trough formed by flexural loading of the Sabah Shelf and adjacent landmass onto the extended continental crust of the Sabah Platform. The geology of the region has been described and discussed by many authors (e.g., Hutchison, 2004, 2010; Franke *et al.*, 2008; Hesse *et al.*, 2009, 2010; Hutchison & Vijayan, 2010).

Offshore NW Sabah is the only place in Malaysia where oil is being produced in deep waters (> 200 m). Oil and gas fields have been discovered in a series of anticlinal structures developed in the upper slope region known as the deepwater fold-thrust belt (DWFTB) on the landward side of the Sabah Trough (Figures 3). This deformed zone with a characteristic stepped bathymetric profile merges with the toe-thrust zone of the Baram Delta to the west and extends for more than 400 km parallel to the Sabah coastline. The fold-thrust anticlines occur as a series of elongate, linear ridges on the seafloor with lengths of about 10-50 km (Figure 3B). They developed in late Miocene-Pliocene sedimentary sequences as fault-propagation folds and fault-bend folds above a major shale decollement assumed to be present beneath the Sabah Shelf sedimentary prism (Morley *et al.*, 2011) (Figure 4). The main thrust fault activity occurred

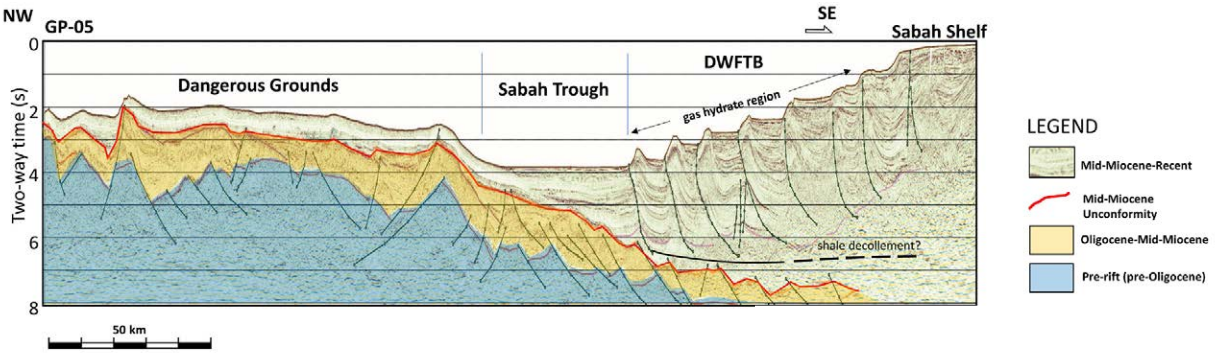

Figure 4: NW-SE seismic profile across the Sabah Shelf to Dangerous Grounds (modified from Vijayan *et al.*, 2013). See Figure 5 for the location of profile. The hydrate deposits discussed in this paper are found on the stepped slopes of the DWFTB formed by NW-verging thrusts in the Neogene sequences down to the flat seafloor of the Sabah Trough (average water depth 2900 m).

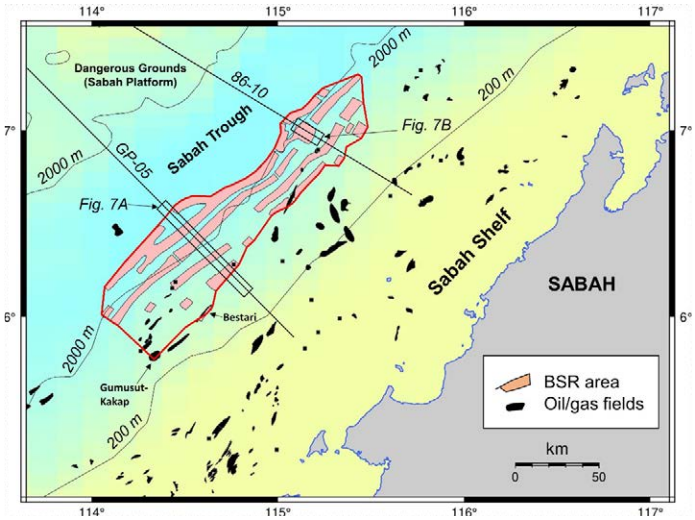

Figure 5: Map of offshore NW Sabah showing the gas hydrate area indicated by BSRs in seismic data (pink polygons based on Behain, 2005). Some of the BSRs occur in areas above proven oil/gas accumulations (black polygons) in subsurface Miocene-Pliocene reservoirs. The red line enveloping the BSR region is considered as the maximum extent of the hydrate field for the purpose of this assessment (12,365 km^2). Gumusut-Kakap field is located at the SW corner of the hydrate field (arrow). The 200 m and 2000 m isobaths are shown to represent the shelf edge and the outline of the Sabah Trough, respectively. The locations of two seismic lines are shown: GP-05 is the regional profile in Figure 4 and a segment of which crosses the hydrate field and is shown in Figure 7A while 86-02 is the BGR profile from which a small segment is shown in Figure 7B.

during Pliocene to Holocene (Hesse *et al.*, 2010). At least nine NW-verging asymmetrical fold-thrust anticlines have been identified in seismic data, with the youngest and widest seaward, near the present-day thrust front, and the oldest and narrowest landward, indicating an overall north-westward (seaward) directed thrust sequence (Hesse *et al.*, 2009). The anticlines are separated by hanging-wall synclines that show landward stratigraphic thickening due to syn-kinematic growth in the hanging-wall strata.

GAS HYDRATE SYSTEMS

Gas hydrate stability

Gas hydrates form at suitable temperature and pressure conditions in the presence of hydrocarbon gas, typically methane. Hydrates may even form at the seabed if bottom water temperatures are cold enough (e.g., <5 °C). They may form throughout the sediment column down to a certain depth when temperatures become too high. The depth to the base of the stability zone is dictated by the geothermal gradient and to a lesser degree by pressure; pressure tends to be high even at the seabed, due to the low temperatures of the deep sea. Below the base of the gas hydrate stability zone (GHSZ) methane may exist as free gas. Hence, at the right seabed temperature gas hydrates may occur within the top-most sediments (i.e., GHSZ). To illustrate the relationship between hydrate phase stability and thickness of GHSZ, Figure 6 shows the phase stability diagram of gas hydrate in a depth-temperature field based on an example from McLeod (1982). Hydrate phase stability is essentially defined by the coincidence of water temperature at the seabed (or seabed temperature) and the gas hydrate-gas phase stability curve based on a pure methane-water system. In principle, any sediment with a temperature below the phase stability curve has the potential to develop gas hydrates. However, the seabed temperature must be low enough for gas hydrates to form; this is determined by the water temperature-depth curve. The minimum temperature at which this may occur is

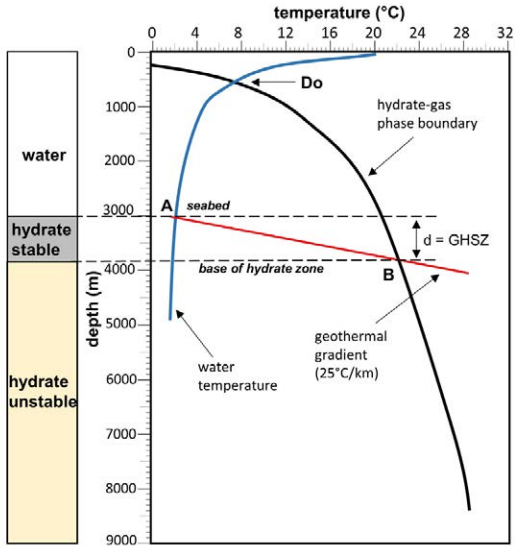

Figure 6: Hydrate stability phase diagram to illustrate the determination of the thickness of the gas hydrate stability zone (GHSZ). Modified and redrawn from McLeod (1982). The determination is based on the intersection points of the geothermal gradient (red line, assumed to be linear and constant) with the water/seabed temperature profile (blue curve) and the hydrate-gas phase boundary (black curve). In this example, for a seabed at 3000 m water depth (point A) and geothermal gradient of 25 °C/km the base of the GHSZ would be at 3800 m (point B). The thickness, *d*, of the GHSZ is given by the vertical separation between A and B.

given by the intersection of the hydrate phase stability curve and the water temperature curve (depth D_o, Figure 6). Thus, for the specific case shown in Figure 6, gas hydrate may start to form in the sediments at the seabed in water depths of about 600 m where the seabed temperature is about 7 °C. Note however, since the seabed depth D_o is at the threshold of the hydrate stability field, the thickness of the GHSZ at that depth would be almost zero. More hydrates would form at greater water depths and at lower temperatures than at D_o.

At any seabed depth greater than D_o, the thickness of the GHSZ (i.e., the interval between the seabed and the base of the GHSZ) may be estimated by plotting the temperature profile of the sediments, which is essentially the geothermal gradient, on the phase stability diagram. For example, in Figure 6, beneath the seabed at 3000 m water depth, the geothermal gradient is 25 °C/km (red line). The intersection of the geothermal gradient line with the hydrate phase boundary defines the base of the GHSZ, from which the thickness of the GHSZ is determined. Figure 6 also indicates that a lower geothermal gradient (steeper red line) would result in a deeper phase boundary between hydrate and free gas in the sediment, and hence a thicker GHSZ. Conversely, there are areas where the geothermal gradient is too high to sustain the formation and preservation of hydrates in the sediment.

Bottom-simulating reflectors

The gas hydrate stability zone (GHSZ) in marine areas is usually detected on seismic reflection data by the presence of bottom-simulating reflectors (BSR), which are essentially high-amplitude, reverse-polarity reflectors occurring at ~250-350 ms (~250-500 m) below the seafloor. They represent reflections from the interface of a sediment-hosted hydrate layer with free gas trapped in sediment directly below it. A BSR represents the phase boundary between hydrate-bearing sediments (high P-wave velocity) and the underlying free-gas bearing sediments (lower P-wave velocity). The high velocity contrast, due to either the hydrate-to-free gas boundary or hydrate to water-saturated sediment boundary, produces a significant negative acoustic impedance contrast, which results in a strong reflection surface (Kvenvolden, 1993; Holbrook *et al.*, 1996). Besides the methane trapped as hydrates, methane and other hydrocarbon gases occur in the gaseous phase (free gas) below the GHSZ, where temperatures are above the threshold for hydrate formation (Figure 6). The GHSZ also effectively acts as an impervious barrier to fluid migration and, where there is structural closure, a seal below which free gas can accumulate.

BSRs are generally parallel to the seabed reflection (hence, the name) because the lower limit of hydrate formation is governed by pressure and temperature conditions and not geologic conditions. As a result, BSRs may be discordant with the sedimentary layering depending on the local seabed topography, subsurface structure, and stratigraphy. Although BSRs are commonly used as an indicator of gas hydrates in contact with free gas trapped beneath, it has been shown that their absence does not necessarily imply absence of hydrates, as it likely also depends on the hydrate/gas saturation and the resultant impedance contrast at that interface. Some studies have shown that gas hydrates also commonly occur outside BSR regions which suggests that hydrates are more widespread than can be detected by seismic alone (e.g., Majumdar *et al.*, 2016; Cook & Portnov, 2022).

In the Sabah margin, BSRs are commonly observed within the crests of fold-thrust anticlines that make up the

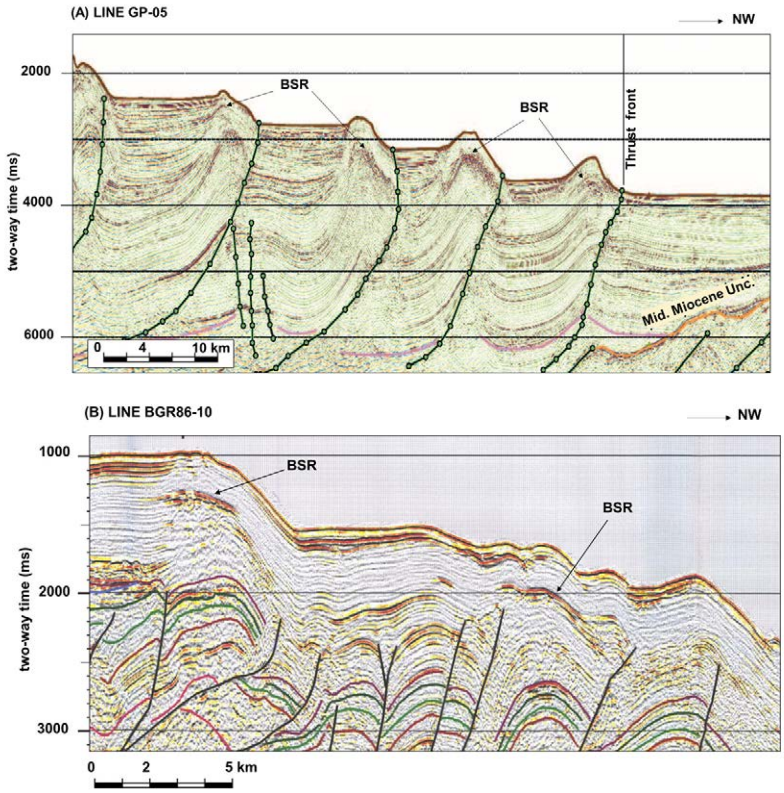

Figure 7: Examples of bottom-simulating reflectors (BSR) from offshore Sabah. Both lines cross the DWFTB from SE to NW (for line locations, see in Figure 5). (A) Part of deep seismic profile GP-05 showing BSRs at the crests of fold-thrust structures (modified from Vijayan *et al.*, 2013). (B) Part of seismic line BGR86-10 showing BSRs below some seabed features (modified from Madon *et al.*, 2015).

DWFTB (Figure 7). Those anticlinal crests are also drilling targets within the prolific middle Miocene-Pliocene section. As explained above, a BSR is caused by the impedance of free gas beneath hydrate. It is known that gas migrates up section along permeable pathways. The strong BSR observed at the crests of anticlines (Figure 7) is therefore due to the abundance of thermogenic gases migrating from below. As the BSR is normally considered as a proxy for the base of the GHSZ in marine sediments, its depth provides a means for estimating the potential thickness of hydrate deposits. The depth of the BSR may also be used to estimate heat flow in marine areas where direct heat flow probe measurements are not available. Such estimation can be made because, assuming hydrostatic conditions, the depth of the BSR is also a function of the thermal gradient (Ohde *et al.*, 2018).

SABAH GAS HYDRATES

Based on their known stability field, gas hydrates are expected to occur in the deepwater regions of Sarawak and Sabah in NW Borneo where seabed temperatures at water depths greater than 1000 m can be as low as 2 – 4 °C (Figure 8). To date, however, gas hydrates have only been reported in the deepwater Sabah area, particularly from the DWFTB on the landward side of the Sabah Trough (Figure 5). The first observation of a BSR was in one of the earliest deepwater seismic surveys (BGR-86) (Hinz *et al.*, 1989). Subsequently, other workers reported BSRs from the same region using this dataset (Gee *et al.*, 2007; Hesse *et al.*, 2009, 2010). A dataset acquired later by BGR in 2001 (BGR-01) also showed the presence of BSR between 250 and 350 m below the seafloor in the fold-thrust belt area (Behain *et al.*, 2003; Behain, 2005; Franke *et al.*, 2008). More recent works have also mentioned or reported the presence of BSR and/or gas hydrates in offshore NW Sabah (e.g., Warren *et al.*, 2010; Laird & Morley, 2011; Dan *et al.*, 2014; Paganoni *et al.*, 2016, 2018; Goh *et al.*, 2017; McGiveron & Jong, 2018; Jong *et al.*, 2020; Wu *et al.*, 2020).

The most detailed mapping of hydrate distribution in offshore NW Sabah was by Behain (2005) who examined in detail the 1986 and 2001 seismic data from BGR and mapped the locations of BSRs across almost the entire length of the DWFTB. Behain's BSR map was published by Hesse *et al.* (2010) and is reproduced in Figure 5. Most of the BSRs are observed within the crests of the fold-thrust anticlines, which form long curvilinear ridges on the seabed as well as within the subsurface Miocene-Pliocene sediments underneath the stepped continental slope on the landward side of the Sabah Trough. Hesse *et al.* (2010) reported that BSRs are widespread in fold-thrust anticlines below water depths of 2600 m. The amplitude of the BSR generally decreases with distance from the anticlinal crests. Similar features are observed in neighbouring offshore Brunei where AVO studies indicated that the free gas column can be as thick as 250 m below the BSR (Laird & Morley, 2011).

Besides the BSRs mapped by Behain (2005), gas hydrates were also reported from the inner slopes of the Sabah Trough at the Gumusut-Kakap (water depth range 900 – 1200 m) (Hadley *et al.*, 2008; Paganoni *et al.*, 2016) and Bestari (~1100 – 1150 m) deepwater fields (McGiveron & Jong, 2018) (see Figure 5 for location). Both these hydrocarbon-bearing structures are older, buried fold-thrust anticlines within the same trend as the DWFTB and do not have significant bathymetric expression. At Bestari, the presence of a BSR with its base between 120 and 140 m depth below the seafloor was used to estimate the geothermal gradient at that location (77 – 82 °C/km) (McGiveron & Jong, 2018). An estimated 33.7 m thickness of gas hydrates were encountered in the wells (Goh *et al.*, 2017; Jong *et al.*, 2020).

GHSZ thickness

The thickness of the GHSZ in the Sabah hydrate field was estimated using the stability field of pure methane in sea water (Sloan, 1998), given by the following equation that relates the temperature of the hydrate phase boundary, T_h, with depth, *z*, in hydrostatic subsurface conditions:

$$T_h = 8.9 \ln (z) - 50.1 \quad (1)$$

From the seabed temperature-depth data for NW Borneo (Figure 8A) an approximate relationship between seabed temperature (T_s) and water depth (*z*) across the hydrate field was derived as a power law of the form:

$$T_s = Az^B \quad (2)$$

where the constants are A= 300 and B = -0.5719.

Figure 9 shows the two curves described by equations 1 and 2. The point of intersection between the two curves represent the conditions under which gas hydrates are expected to form. This depth D_o in Figure 6 is determined to be in a water depth of about 640 m in the Sabah area, corresponding to an average seabed temperature of about 7.4 °C (Figure 9). As the map in Figure 8B shows, most of the deepwater areas offshore Sarawak and Sabah where water depths are greater than about 650 m are likely to have the right temperature for gas hydrates to form. To estimate the thickness of the GHSZ, an average geothermal gradient of 62.5 °C/km was assumed for the Sabah Trough area (Madon & Jong, 2021) and the geothermal gradient line is plotted through selected water depths on the seabed-temperature curve. The base of the GHSZ relative to the seabed is represented by the intersection of the geothermal gradient line with the hydrate stability curve from which the thickness *d* is derived. Several geothermal gradient lines representing selected values of seabed depth are shown in Figure 9 where the corresponding GHSZ thicknesses are determined. Since the hydrate stability curve is based on a logarithmic equation (eq. 1), the

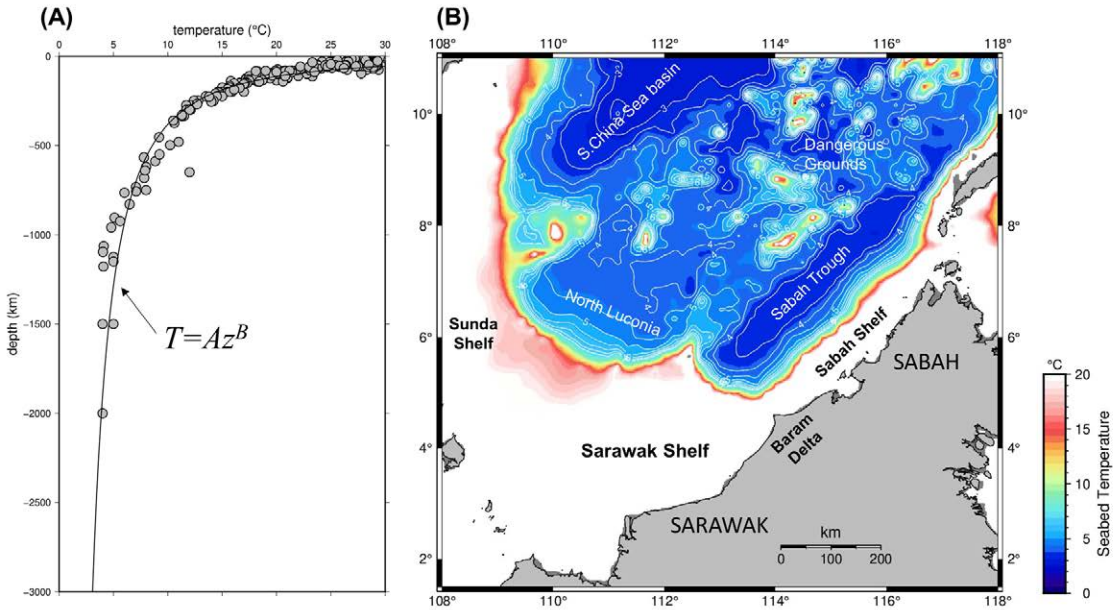

Figure 8: Seabed temperature variation with water depth in offshore NW Borneo. (A) Plot of data compiled by Shell mainly from offshore Sabah and Sarawak showing the exponential decrease of temperature with water depth to approximately 4 °C below 1500 m. (Data from Madon & Jong, 2021). The seabed temperature-depth (*T-z*) relationship is approximated by a power law of the form $T = A.z^B$, where A= 300 and B = -0.5719. (B) Map of seabed temperature offshore NW Borneo calculated from satellite-derived bathymetry from Sandwell & Smith's grid ver. 3.01 using the power law curve in A. To emphasise the deepwater areas, only temperatures between 0 and 20 °C are plotted. The map shows that the entire deepwater area (blue area beyond the shelf-edge) has seabed temperatures of less than about 7 – 8 °C.

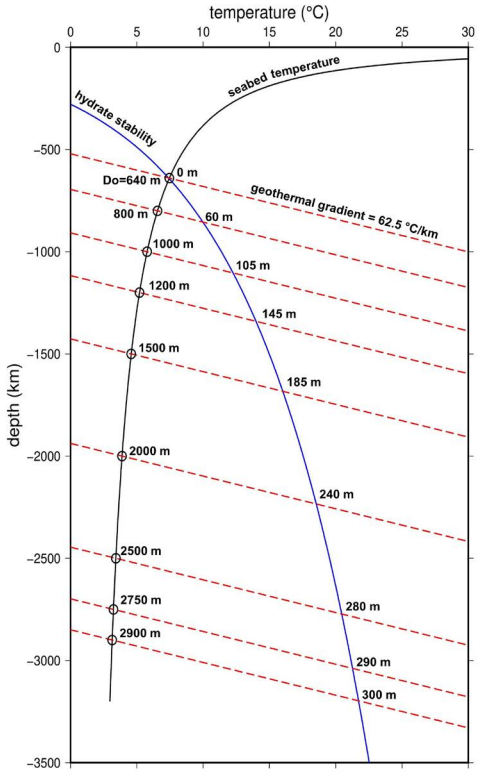

Figure 9: Gas hydrate stability chart for offshore NW Sabah. Blue curve is gas to gas-hydrate phase boundary based on pure methane and water (Sloan, 1998). Black curve is seabed temperature vs depth curve based on data from NW Borneo (Figure 8A). Red dashed lines are average geothermal gradient lines (62.5 °C/km) drawn through selected seabed depths (on the black curve) and projected to the phase boundary curve (blue curve). The intersection points represent the depth of the base of GHSZ relative to the seabed depth.

thickness of the GHSZ also behaves in a logarithmic manner (Figure 10), given by:

$$d = 193.94 \ln (z) - 1239 \quad (3)$$

which describes the relationship between the thickness of the GHSZ, *d*, and water depth, *z*. Clearly, a different geological setting with a different geothermal gradient would require a different equation to be established. For the specific value of geothermal gradient (62.5 °C/km), equation 3 was used to calculate the GHSZ thickness directly from water depth *z*.

Figure 10 shows that the thickness of the hydrate stability zone ranges from zero at a water depth of 640 m to 300 m at 2900 m, which is the base of the Sabah Trough. These estimates of GHSZ thickness will be used in the calculation of total gas resource from the hydrates, as described below.

RESOURCE ESTIMATION

With a method to determine the thickness of GHSZ established, the volume of *in situ* gas hydrate deposits may be estimated using the same principles commonly used in conventional hydrocarbon resource assessment. The estimated *in situ* hydrate volume can easily be converted to the volume of methane at standard temperature and pressure (STP) conditions at the surface by applying the standard "gas expansion factor", B_g.

Basic formula

The basic equation for the volume (V) of gas initially in place (GIIP) at standard temperature and pressure (STP) in billion cubic feet (BCF) is given by the product of three basic parameters:

$$V_{GIIP} = A \cdot N_p \cdot Y \quad (4)$$

where A is the areal extent of the hydrate deposit (or field) in m^2, N_p is net pay thickness, and Y is the "yield" which is the effective productivity of the hydrate reservoir/field measured as the volume of methane at STP per unit volume of hydrate at subsurface conditions (BCF/m^3). N_p is the product of the thickness of the GHSZ, *d*, in metres, and the net-to-gross ratio of reservoir to non-reservoir, N_g. The quantity Y is analogous to "million cubic feet per acre-ft" in conventional hydrocarbon assessments (Rose, 2001). It is considered as a measure of the "gross productivity" of the hydrate reservoir which, as in conventional hydrocarbons, is principally governed by porosity (Φ) and hydrate saturation (S_h):

$$Y = \Phi \cdot S_h \cdot B_g \cdot C_o \cdot (35.315 \times 10^{-9}) \quad (5)$$

B_g is the ratio of the volume of methane at STP per unit volume of hydrate at reservoir conditions, and a value of 164 is normally used (e.g., Wang & Lau, 2020; Zhang *et al.*, 2021). C_o is the cage occupancy of methane in hydrates, which is generally and relatively high (>0.96) in the Shenhu hydrate deposits in the Pearl River Mouth Basin and in the Nankai Trough hydrates, southern Japan (Fujii *et al.*, 2015). For this study, a C_o of 0.96 was used. The constant 35.315×10^{-9} BCF/m^3 is the unit conversion factor from cubic metres to billion cubic feet (BCF), which is the unit volume for gas commonly used in the petroleum industry.

Table 1 lists the values of the key parameters for the Sabah hydrates based on the current study and Jong *et al.* (2020). For comparison, data from other major hydrate provinces were also listed, namely the Shenhu hydrate field in the Pearl River Mouth Basin, northern South China Sea margin, the Nankai Trough south of Honshu Island, Japan, and offshore Newfoundland and Labrador Sea, Canada. These data are useful as analogues to guide the selection of appropriate parameter values for the calculations.

Deterministic estimation

The volume of methane from the gas hydrates was estimated deterministically using equation 4 with the

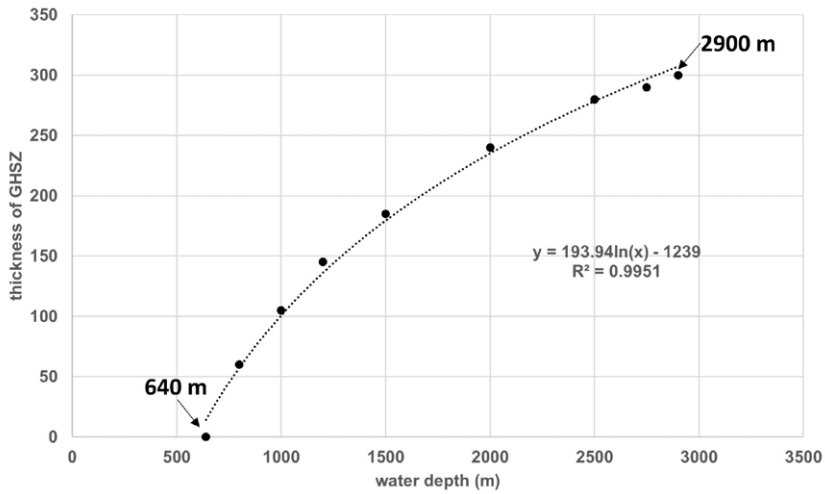

Figure 10: Relationship between water depth and thickness of GHSZ based on the corresponding pairs of intersecting points in Figure 9. The regression line is equation 3 which is used to predict the GHSZ thickness for a given water depth.

Table 1: Basic reservoir parameters from the Sabah hydrates compared with other hydrate fields.

Parameters	Malaysia (Sabah)	Northern South China Sea margin (Shenhu)	Japan (Nankai Trough)	Canada (offshore Newfoundland and Labrador sea)
Water depth (m)	640-2900	1105-1423	857-1405	620-2850
Seabed temperature (°C)	4.5	3.38–4.58	3.5	2-4
Geothermal gradient (°C/km)	62.5	43.65–67.60	40	32
BSR depth below seabed (m)	250-360	170-242	278-315	250-445
Thickness of hydrate zones (m)	33.7	10-43	14-33	65-80; ave. 79
Porosity (%)	45-65; ave. 55	30-50	34-50	34-46
Saturation (%)	62.5-83.5; ave. 73.7	20.5-23.0% (core data)	35-80	2-6 (up to 38)
Net-to-gross (%)	26	-	28-60	-
Occupancy (%)	96	86-99	94	29-54
Source of methane	Biogenic and thermogenic	Biogenic, minor thermogenic	Biogenic	Biogenic or thermogenic
References	Behain, 2005; McGiveron & Jong, 2018; Jong *et al*., 2020.	Liu *et al*., 2012; Su, M. *et al*., 2016; Su, P. *et al*., 2022.	Fujii *et al*., 2009; 2015; Yu *et al*., 2019.	Majorowicz & Osadetz, 2001; Mosher, 2008; 2011.

appropriate values chosen for the parameters based on the available data. Table 2 (column 2) lists the values chosen for the calculations. The total area where BSRs were identified, as mapped by Behain (2005) and shown by the ribbon-shaped polygons in Figure 5, are taken as the "proven" hydrate area, which is 3245 km^2. The average water depth within the red envelope of the hydrate field in Figure 5 is 1761 m. Using equation 3 this gives the average thickness of the GHSZ zone of 210 m. No information is available on the actual hydrate thickness, except that Jong *et al.* (2020) reported 33.7 m of hydrate thickness in the Bestari field in water depths of about 1150 m. Since the expected GHSZ thickness at this water depth is 128 m (equation 3), 33.7 m is about 26% of the gross thickness. Thus, N_g is given a value of 0.26 in the calculation.

In Figure 11A, porosity data from ODP leg 184 site 1143 in the South China Sea down to 500 m below the seafloor indicate that porosity decreases from 80% to 50%. Based on this dataset of 400 measurements the average porosity for the top 400 m of deep-sea sediments is 63% (Figure 11B). The generally high porosities in the distribution indicate that the entire sediment column may be considered as a potential hydrate reservoir, depending on the N_g. For the current assessment, however, a more conservative range of porosities was adopted, based on the reported values in the Shenhu area (30% – 50%) (Table 1). An average of 40% is used in the calculation.

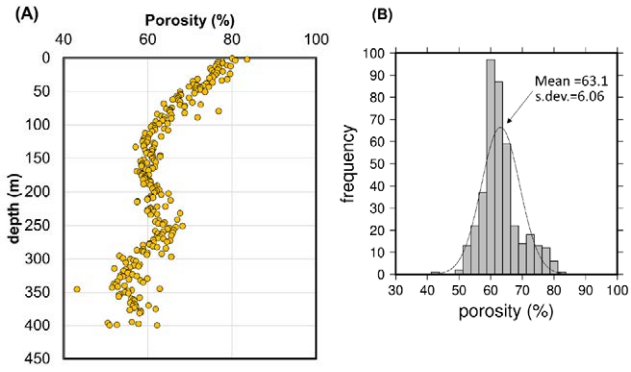

Figure 11: Porosity data from ODP leg 184 site 1143 in the South China Sea, used as rationale for choosing the input parameters in the resource estimation. (A) Porosity-depth profile showing a range of porosities between about 50% and 80% in the topmost 400 m of oceanic sediments. (B) Histogram of the porosity data in A showing a generally normal distribution with a mean of 63.1% and standard deviation of 6.06%.

For gas hydrate saturation, S_h, values quoted in the literature are highly variable (Table 1). In the Nankai Trough, offshore Japan, hydrate saturations may be up to 35% (Miyakawa *et al.*, 2014), while in the North Slope test well, off Alaska, gas hydrate saturations can be as high as 80% (Haines *et al.*, 2020). In the study area, Behain (2005) determined that up to 9% of the pore space in the GHSZ are filled with gas hydrates. This value seems to be on the low

Table 2: Resource estimation for Sabah hydrates. GIIP – Gas Initially In Place, EUR – Estimated Ultimate Recovery, BCF – billion cu. ft., TCF – trillion cu. ft. * - The dimensionless quantity B_g is the ratio of volume at STP per unit volume at reservoir conditions.

Parameter	DETERMINISTIC	PROBABILISTIC			
		P90	P50	MEAN	P10
Area, A (km^2)	3,245	3,245	6,344	7,129	12,365
Thickness, *d* (m)	210	170	206	208	250
Net-to-gross ratio, N_g	0.26	0.11	0.26	0.31	0.60
Net pay, N_p (m)	54.6	22	52.2	61.3	120
Porosity, f (fraction)	0.40	0.30	0.38	0.39	0.50
Saturation, S_h (fraction)	0.23	0.20	0.40	0.45	0.80
Gas expansion ratio, B_g*	164	158	163.9	164	170
Cage occupancy, C_o	0.96	1.0	1.0	1.0	1.0
GIIP (BCF)	90,629	72,829	251,958	364,416	851,882
GIIP (TCF)	91	73	252	364	852
GIIP (10^9 m^3)	2,566	2,062	7,135	10,319	24,123
EUR (TCF)	27	22	76	109	256
EUR (10^9 m^3)	770	619	2,140	3,096	7,237

side relative to those reported from other localities. While Goh *et al.* (2017) quoted a value of more than 60% for Sabah, Mosher (2011) used a range from 2-6% in offshore Newfoundland. On the other extreme, in the Bay of Bengal saturations reached 65%–85% of the pores in sandy reservoir sediments while clayey interlayers between the reservoir sediments had hydrate saturations near 10%, suggesting lithofacies control on hydrate saturation (Holland *et al.* 2019). The values quoted for the Nankai and Shenhu areas are intermediate and perhaps more reasonable for Sabah (Table 1). According to Wang *et al.* (2011), core-derived data from the Shenhu area, South China Sea, indicate 10-45% saturation at depths of 190–221 m below the seafloor. Based on this information, gas hydrate saturation ranges from 20% to as high as 80%. For the calculation, a conversative value of 23% was used based on the core data from Shenhu hydrate field (Table 1). A cage occupancy (C_o) of 0.96 was used (Jong *et al.*, 2020). Based on the above parameters, the estimated methane resource initially in place (V_{GIIP}) at STP is 90,629 BCF (2.566 x 10^{12} m^3).

Probabilistic estimation

To account for the large uncertainties in the parameters, a probabilistic estimation was also carried out by assigning a probability distribution to each of the input parameters in Table 2. As commonly done in conventional oil and gas resource estimation, a lognormal distribution is assumed for all parameters, the product of which will also be lognormal (Rose, 2001). A characteristic and useful feature of lognormal distributions is that the total population can be described by specifying only two values within the range of all possible values between P1 (absolute maximum) and P99 (minimum)[2]. In practice, for each parameter, a high-case ("reasonable maximum") and a low-case ("reasonable minimum") estimate were determined as proxies to the P10 and P90 values, respectively, while the median (P50) and mean or "most likely" values were calculated from the lognormal probability distributions generated through a Monte Carlo simulation.

Table 2 (columns 3 to 5) lists the relevant parameters for the probabilistic resource estimation. For the purpose of this estimation, the total BSR area of 3,245 km^2 is considered as the minimum "proven" area (P90). If it is assumed that the GHSZ is continuous throughout the intervening areas between the BSRs, the red line envelope surrounding the mapped BSR areas can be used as the proxy for the maximum (P10) area (Figure 5). This value is 12,365 km^2 (Table 2).

The thickness of GHSZ, *d*, is considered as the "gross thickness" of potential hydrate reservoir. As determined above, the GHSZ zone ranges from zero at 640 m water depth to 300 m at 2900 m water depth on the flat seafloor of the Sabah Trough. Slightly greater numbers were estimated by Behain (2005) (up to 360 m in the Sabah Trough), probably due in part to his use of a lower geothermal gradient (60 °C/

[2] By convention, a Px value represents the value for which there is a x% probability that the resource volume is greater or equal to that value.

km). The value of 300 m is considered a more conservative and reasonable maximum thickness for the GHSZ. For the Monte Carlo simulation a low and high values of 170 m and 250 m were used, based on the Shenhu data (Table 1). Assuming a reasonable range of N_g between 0.11 and 0.60, the corresponding range for net pay thickness is 22 – 120 m. Based on these parameter ranges, the results of the Monte Carlo simulation are given at the bottom of Table 2. The results indicate that the P50 estimate for the total methane resource (GIIP) from the Sabah gas hydrates ranges from 72 to 852 TCF (2.06 – 24.1 x 10^{12} m^3) with a mean of 364 TCF (10.3 x 10^{12} m^3) and a P50 value of 252 TCF (7.1 x 10^{12} m^3). Assuming a 30% recovery factor (based on Shenhu data), the corresponding EUR estimates are 22 – 256 TCF (0.619 – 7.237 x 10^{12} m^3) with a mean of 109 TCF (3.1 x 10^{12} m^3) and a P50 of 76 TCF (2.1 x10^{12} m^3).

DISCUSSION

Resource estimation

Since gas hydrates may also exist in the absence of a BSR, the above estimates of the potential gas resource should be regarded as conservative. The estimated GIIP may seem large, but it is realistic considering the large area of the hydrate field (Figure 5). It is important to emphasise that the GIIP volume is the quantity of gas originally in place in the subsurface reservoirs that is potentially available to be exploited. The actual quantity of gas that is technically recoverable from those reservoirs is unknown and yet to be determined. In conventional hydrocarbon assessments, the proportion of recoverable hydrocarbons is estimated by applying a recovery factor (RF) to the GIIP. RF varies according to geological situations; in practice they may be as high as 35% for oil reservoirs and 70% for gas reservoirs (e.g., Shepherd, 2009). Since there is no commercial exploitation of gas hydrates anywhere, RF has to be derived either by analogy with conventional reservoirs or by physical and numerical simulations (e.g., Konno *et al.*, 2014). Based on the latter approach, Zhang *et al.* (2021) quoted RF values ranging between 15% and 70% and an average of 30%. Using this average value, the estimated ultimate recoverable (EUR) volume for the Sabah hydrates (P50) of 76 TCF (2.1 x10^{12} m^3). In the northern South China Sea, the estimated recoverable resource for the Shenhu deposit, assuming an average RF of 30%, is ~250 TCF (7.0×10^{12} m^3) (Zhang *et al.*, 2021), which is 3.3 times larger than the Sabah hydrate deposit. As another comparison, the Hikurangi hydrate deposit in offshore New Zealand, which is spread over an area of 50,000 km^2 has been estimated to hold a potentially recoverable gas resource of 20 TCF (Pecher & Henrys, 2003).

A major uncertainty in the estimation of gas hydrate resource is the distribution of hydrates in the subsurface. While in conventional hydrocarbons the distinction between reservoir and non-reservoir is easily recognised by applying a variety of cut-offs (e.g., porosity, shale volume), in the case of gas hydrates it is unclear what proportion of the estimated gas volume reside in porous sands and silts as opposed to the whole sediment column within the GHSZ. Data from the Shenhu area suggests that the highest hydrate reserves are in clayey silt reservoirs (Ye *et al.*, 2020) whereas in the Cascadia margin, NE Pacific, there appears to be a preference for hydrates to form in the coarse-grained sediments (Riedel *et al.*, 2006; Torres *et al.*, 2008).

Results from IODP legs 204 and 311 in the Cascadia margin show significant variations in gas hydrate concentration in the GSHZ (Tréhu *et al.*, 2003, 2004). At some localities on the Cascadia margin, gas hydrate concentrations clearly increase towards the base of the GHSZ, while in others no clear depth trends in the gas hydrate concentrations were observed (Torres *et al.*, 2008). Geological conditions may influence hydrate concentrations; for example, it was found that where hydrothermal gas venting occurs hydrate concentrations can be as much as 25% within the top tens of metres of sediments (Tréhu *et al.*, 2004). Such a large uncertainty in gas hydrate distribution justifies a conservative approach in resource estimation.

It is noted that the Sabah gas hydrate deposits occur over a large area; the P10 value for the area of the Sabah hydrate field is 12,365 km^2. In calculating the upside potential, it was assumed that the gas hydrate deposits are evenly distributed across the entire area within the BSR region while the probabilistic approach takes into account all possible outcomes within the range of input parameters. This estimate is a first attempt and should be improved with more data and a greater understanding of the hydrate occurrences and their distribution. The assumptions in the input parameters should also be reviewed as more information becomes available. It should be noted also, as mentioned above, the seabed within the entire deepwater area beyond the 650 m isobath is likely to host gas hydrates. Detailed mapping with high resolution 3D seismic data would help distinguish highly prospective areas from riskier ones. The Sabah hydrate field considered in this study is less than 4% of the total deepwater area within Malaysia's Exclusive Economic Zone. Hence, there is significant potential for exploitation of the gas hydrate resource in the future when the exploitation technologies are mature and appropriate environmental protection measures are in place for such activities to take place. Successful production tests and recoveries of hydrate methane from wells in the Nankai Trough, Japan (Yamamoto *et al.*, 2019; Yamamoto, 2022) as well as in the Shenhu area, northern South China Sea margin (Zhang *et al.*, 2018; Ye *et al.*, 2020) suggest that that future may not be too far away.

Free gas beneath GHSZ

Given the appropriate seabed temperature and geothermal gradient, the formation of gas hydrates in deep-sea sediments also depends on the availability of gas (principally, methane) in the sediment, permeability

pathways that allow gas to enter the hydrate stability zone, and porosity to host the hydrate. Marine sediments are generally expected to generate methane through biogenic activity of microorganisms. Thermogenic gases generated from sediments at greater depths can also rise toward the surface to form hydrate at the appropriate stability conditions or can be trapped as free gas beneath the GHSZ. A strongly reflective BSR is due to a high reflection coefficient at the base of the BSR, and is usually taken as an indication of the presence of free-gas saturated sediment below the GHSZ. Since conventional oil/gas resources in the Sabah Basin are proven (Figure 5), there is no lack of hydrocarbon source for the gas hydrates to form when the subsurface conditions are suitable.

Behain (2005) determined that the strength (amplitude) of the BSRs is a function of the amount of free gas beneath the GHSZ, which results in a strong impedance contrast (higher reflection coefficient) at the base of the GHSZ. He determined from the BGR-01 dataset that the amount of free gas beneath the GHSZ is between 0.5% and 4% of the sediment bulk volume. Assuming a 50% porosity, this means that 8% of the pore volume is occupied by methane (S_h=8%). The volume of free gas that can be trapped below the GHSZ is also a function of the trap closure area and other reservoir properties, as normally evaluated in conventional hydrocarbon prospects. A separate exercise is required to estimate the additional resource from free gas in individual traps (prospects) below the GHSZ which may result in a significant addition to the total gas hydrate-related hydrocarbon resource.

CONCLUSIONS

Gas hydrates are commonly found in offshore NW Sabah, especially in the deepwater fold-thrust belt on the landward side of the Sabah Trough. The Sabah hydrate field has the potential to be one of the main gas hydrate resources in the region and will be particularly important as an energy source for Malaysia.

Identification of gas hydrates in the offshore area is mainly through seismic reflection data by way of bottom-simulating reflectors (BSR). The distribution of gas hydrates in the Sabah deepwater fold-thrust belt has been mapped (e.g., Behain, 2005) and was used in the estimation of total gas resource in place (GIIP). The thickness of the GHSZ ranges from zero at 640 m water depth to 300 m at 2900 m water depth in the Sabah Trough.

Based on a probabilistic estimation, the total in-place methane resource (GIIP) potentially available from the Sabah gas hydrates ranges from 72 to 852 TCF (2.06 – 24.1 x 10^{12} m^3) with a mean of 364 TCF (10.3 x 10^{12} m^3) and a P50 value of 252 TCF (7.1 x 10^{12} m^3). How much of this *in situ* resource is actually technically recoverable is uncertain and would depend on factors such as technology, economics and reservoir properties. Further work is required to improve our understanding of the gas hydrate distribution, thicknesses and geochemistry, among others, in order to have a better estimate of the resource potential.

ACKNOWLEDGEMENTS

Useful comments and suggestions received from four anonymous reviewers for GSM helped to improve the paper. I also thank David Mosher for his constructive comments on the draft manuscript.

CONFLICT OF INTEREST

I declare that i do not have any conflict of interest with regard to the contents of this paper.

REFERENCES

Behain, D., 2005. Gas hydrate offshore NW Sabah: Morpho-tectonic influence on the distribution of gas hydrate and estimation of concentration of gas hydrate above and free gas below the Gas Hydrate Stability Zone. Doctoral dissertation. Technical University of Clausthal. 153 p.

Behain, D., Fertig, J., Meyer, H., Franke, D., & Barckhausen, U., 2003. Properties of a gas hydrate province on a subduction-collision related margin off Sabah, NW Borneo. (POPSCOMS). EGS – AGU – EUG Joint Assembly, Abstract 10008. (POPSCOMS). EGS – AGU – EUG Joint Assembly, Abstract 10008.

Birchwood, R., Dai, J., Shelander, D., Boswell, R., Collett, T., Cook, A., Dallimore, S., Fujii, K., Imasato, Y., Fukuhara, M., Kusaka, K., Murray, D., & Saeki, T., 2010. Development of gas hydrates. Schlumberger Oilfield Review, 22(1), 18-33.

Cook, A.E., & Portnov, A., 2022. Natural gas hydrate systems. In: Bell, R., Iacopini, D., Vardy, M. (Eds.), Interpreting seismic data. Elsevier, 17-32. https://doi.org/10.1016/B978-0-12-818562-9.00006-6.

Dan, G., Cauquil, E., & Bouroullec, J.-L., 2014. 3D seismic and AUV data integration for deepwater geohazard assessment: Application to offshore Northwest Borneo, Brunei. Offshore Technology Conference-Asia, Kuala Lumpur, Malaysia, March 2014. Paper Number: OTC-24796-MS. https://doi.org/10.4043/24796-MS.

Franke, D., Barckhausen, U., Heyde, I., Tingay, M., & Ramli, N., 2008. Seismic images of a collision zone offshore NW Sabah/Borneo. Marine and Petroleum Geology, 25(7), 606-624. https://doi.org/10.1016/j.marpetgeo.2007.11.004.

Fujii, T., Nakamizu, M., Tsuji, Y., Namikawa, T., Okui, T., Kawasaki, M., Ochiai, K., Nishimura, M., & Takano, O., 2009. Methane-hydrate occurrence and saturation confirmed from core samples, eastern Nankai Trough, Japan. In: T. Collett, A. Johnson, C. Knapp & R. Boswell (Eds.), Natural gas hydrates—Energy resource potential and associated geologic hazards. AAPG Memoir, 89, 385–400. https://doi.org/10.1306/13201112M893350.

Fujii, T., Suzuki, K., Takayama, T., Tamaki, M., Komatsu, Y., Konno, Y., Yoneda, J., Yamamoto, K., & Nagao, J., 2015. Geological setting and characterization of a methane hydrate reservoir distributed at the first offshore production test site on the Daini Atsumi Knoll in the eastern Nankai Trough, Japan. Marine and Petroleum Geology, 66, 310–322. http://dx.doi.org/10.1016/j.marpetgeo.2015.02.037.

Gee, M.J.R., Uy, H.S., Warren, J., Morley, C.K., & Lambiase,

J.J., 2007. The Brunei slide: A giant submarine landslide on the North West Borneo Margin revealed by 3D seismic data. Marine Geology, 246(1), 9-23. https://doi.org/10.1016/j.margeo.2007.07.009.

Goh, H.S., Jong, J., McGiveron, S., & Fitton, J., 2017. A case study of gas hydrates in offshore NW Sabah, Malaysia: Implications as a shallow geohazard for exploration drilling and a potential future energy resource. National Geoscience Conference, 9-10 October 2017, Hotel Istana Kuala Lumpur.

Grant, C.J., 2005. Sequence boundary mapping and paleogeographic reconstruction: The keys to understanding deepwater fan deposition across the NW Borneo active margin. adapted from oral presentation at 2005 SEAPEX Exploration Conference, Singapore, 5-7 April.

Hadley, C., Peters, D., Vaughan, A., & Bean, D., 2008. Gumusut-Kakap Project: Geohazard characterisation and impact on field development plans. International Petroleum Technology Conference, 3-5 December, Kuala Lumpur, Malaysia. https://doi.org/10.2523/IPTC-12554-MS.

Haines, S.S., Collett, T., Boswell, R., Lim, T., Okinaka, N., Suzuki, K., & Fujimoto, A., 2020. Gas hydrate saturation estimation from acoustic log data in the 2018 Alaska North Slope Hydrate-01 stratigraphic test well. 10th International Conference on Gas Hydrates (ICGH10), Jun 21-26, 2020, Singapore.

Hazebroek, H.P., & Tan, D.N.K., 1993. Tertiary tectonic evolution of the NW Sabah continental margin. Bulletin of the Geological Society of Malaysia, 33, 195-210. https://doi.org/10.7186/bgsm33199315.

Hesse, S., Back, S., & Franke, D., 2009. The deep-water fold-and-thrust belt offshore NW Borneo: Gravity-driven versus basement-driven shortening. Geological Society of America Bulletin, 121, 939-953. https://doi.org/10.1130/B26411.1.

Hesse, S., Back, S., & Franke, D., 2010. The structural evolution of folds in a deepwater fold and thrust belt – A case study from the Sabah continental margin offshore NW Borneo, SE Asia. Marine and Petroleum Geology, 27(2), 442-454. https://doi.org/10.1016/j.marpetgeo.2009.09.004.

Hinz, K., Fritsch, J., Kempter, E.H.K., Mohammad, A.M., Vosberg, H., Weber, J., & Benavidez, J., 1989. Thrust tectonics along the northwestern continental margin of Sabah/Borneo. Geologische Rundschau, 78(3), 705-730.

Holbrook, W.S., Hoskins, H., Wood, W.T., Stephen, R.A., & Lizarralde, D., 1996. Methane hydrate and free gas on the Blake Ridge from vertical seismic profiling. Science, 273(5283), 1840–1843.

Holland, M.E., Schultheiss, P.J., & Roberts, J.A., 2019. Gas hydrate saturation and morphology from analysis of pressure cores acquired in the Bay of Bengal during expedition NGHP-02, offshore India. Marine and Petroleum Geology, 108, 407-423. https://doi.org/10.1016/j.marpetgeo.2018.07.018.

Hutchison, C.S., 2004. Marginal basin evolution: The southern South China Sea. Marine and Petroleum Geology, 21, 1129–1148. https://doi.org/10.1016/j.marpetgeo.2004.07.002.

Hutchison, C.S., 2010. The North-West Borneo trough. Marine Geology, 271, 32–43. https://doi.org/10.1016/j.margeo.2010.01.007.

Hutchison, C.S., & Vijayan, V.R., 2010. What are the Spratlys? Journal of Asian Earth Sciences, 39, 371-385. https://doi.org/10.1016/j.jseaes.2010.04.013.

Ingram, G.M., Chisholm, T.J., Grant, C.J., Hedlund, C.A., StuartSmith, P., & Teasdale, J., 2004. Deepwater North West Borneo: Hydrocarbon accumulation in an active fold and thrust belt. Marine Petroleum Geology, 21, 879–887. https://doi.org/10.1016/j.marpetgeo.2003.12.007.

Jong, J., Goh, H.S., McGiveron, S., & Fitton, S., 2020. A case study of natural gas hydrates (NGH) in offshore NW Sabah: Identification, shallow geohazard implication for exploration drilling, extraction challenges and potential energy resource estimation. Bulletin of the Geological Society of Malaysia, 70, 57 – 75. https://doi.org/10.7186/bgsm70202005.

Konno, Y., Jin, Y., Shinjou, K., & Nagao, J., 2014. Experimental evaluation of the gas recovery factor of methane hydrate in sandy sediment. RSC Adv., 4(93), 51666-51675. https://doi.org/10.1039/C4RA08822K.

Krey, V., Canadell, J.G., Nakicenovic, N., & 15 others, 2009. Gas hydrates: Entrance to a methane age or climate threat? Environ. Res. Lett., 4(034007), 6 p. https://doi.org/10.1088/1748-9326/4/3/034007.

Kvenvolden, K.A., 1993. Gas hydrates—Geological perspective and global change. Rev. Geophys., 31, 173–187. https://doi.org/10.1029/93RG00268.

Kvenvolden, K.A., 1999. Potential effects of gas hydrate on human welfare. Proc. Natl. Acad. Sci. USA, 96, 3420–3426. https://doi.org/10.1073/pnas.96.7.3420.

Laird, A.P., & Morley, C.K., 2011. Development of gas hydrates in a deep-water anticline based on attribute analysis from three-dimensional seismic data. Geosphere, 7(1), 240–259. https://doi.org/10.1130/GES00598.1.

Liu, C., Ye, Y., Meng, Q-G., & 8 others, 2012. The characteristics of gas hydrates recovered from Shenhu Area in the South China Sea. Marine Geology, 307-310, 22-27. https://doi.org/10.1016/j.margeo.2012.03.004.

Lu, S.-M., 2015. A global survey of gas hydrate development and reserves: Specifically in the marine field. Renewable and Sustainable Energy Reviews, 41, 884–900. https://doi.org/10.1016/j.rser.2014.08.063.

Madon, M. & Jong, J., 2021. Geothermal gradient and heat flow maps of offshore Malaysia: Some updates and observations. Bulletin of the Geological Society of Malaysia, 71, 159-183. https://doi.org/10.7186/bgsm71202114.

Madon, M., Norazlina, J., Ayub, A., Nor Kartini Suriati, M., Najmi, S.M., Ahmad Zamzamie, I., & Azhar, Y., 2015. Structural evolution of the NW Sabah Deepwater fold-and-thrust belt and its implications for hydrocarbon prospectivity. Asia Petroleum Geoscience and Exhibition (APGCE) 2015, 12-13 October, Kuala Lumpur. Proceedings and Abstracts.

Majorowicz, J., & Osadetz, K.G., 2001. Gas hydrate distribution and volume in Canada. AAPG Bulletin, 85(7), 1211–1230. https://doi.org/10.1306/8626CA9B-173B-11D7-8645000102C1865D.

Majumdar, U., Cook, A.E., Shedd, W., & Frye, M., 2016. The connection between natural gas hydrate and bottom-simulating reflectors. Geophys. Res. Lett., 43, 7044–7051. https://doi.org/10.1002/2016GL069443.

Maslin, M., Owen, M., Betts, R., Day, S., Jones, T.D., & Ridgwell, A., 2010. Gas hydrates: Past and future geohazard? Philosophical Transactions of the Royal Society of London A: Mathematical, Physical and Engineering Sciences, 368(1919), 2369-2393.

McGiveron, S., & Jong, J., 2018. Complex geothermal gradients and their implications, deepwater Sabah, Malaysia. Bulletin of the Geological Society of Malaysia, 66, 15 – 23. https://doi.org/10.7186/bgsm66201803.

McLeod, M.K., 1982. Gas hydrates in ocean bottom sediments. AAPG Bull., 66(12), 2649-2662. https://doi.org/10.1306/03B5AC8C-16D1-11D7-8645000102C1865D.

Mienert, J., Tréhu, A.M., Berndt, C., Camerlenghi, A., Liu, C.-S., & Massironi, M., 2022. Finding and using the world's gas hydrates. In: Mienert, J., Christian Berndt, Anne M. Tréhu, Angelo Camerlenghi, & Char-Shine Liu (Eds.), World atlas of submarine gas hydrates in Continental Margins. Springer, Cham, Switzerland. 514 p. https://doi.org/10.1007/978-3-030-81186-0_3.

Miyakawa, A., Saito, S., Yamada, Y., Tomaru, H., & Kinoshita, M., 2014. Gas hydrate saturation at Site C0002, IODP Expeditions 314 and 315, in the Kumano Basin, Nankai trough. Island Arcs, 23(2), 142-156. https://doi.org/10.1111/iar.12064.

Morley, C.K., King, R.C., Hillis, R., Tingay, M., & Backe, G., 2011. Deepwater fold and thrust belt classification, tectonics, structure and hydrocarbon prospectivity: A review. Earth-Science Reviews, 104, 41–91. https://doi.org/10.1016/j.earscirev.2010.09.010.

Mosher, D.C., 2008. Bottom simulating reflectors on Canada's East Coast Margin: Evidence for gas hydrate. Proceedings of the 6th International Conference on Gas Hydrates (ICGH 2008), Vancouver, British Columbia, CANADA, July 6-10, 2008.

Mosher, D.C., 2011. A margin-wide BSR gas hydrate assessment: Canada's Atlantic margin. Marine and Petroleum Geology, 28, 1540 – 1553. https://doi.org/10.1016/j.marpetgeo.2011.06.007.

Nurfadhila, M.S., Ahmad Shamsul Kamal, & Anuar A. Aziz, 2018. Gas hydrate potential in Malaysia – Catching up to compete with shale gas potential in Malaysia. AAPG Asia Pacific Region GTW, Bangkok, Thailand, September 26-27, 2018. AAPG Datapages/Search and Discovery Article #90331.

Ohde, A., Otsuka, H., Kioka, A., & Ashi, J., 2018. Distribution and depth of bottom-simulating refectors in the Nankai subduction margin. Earth, Planets and Space, 70:60. 20 p. https://doi.org/10.1186/s40623-018-0833-5.

Paganoni, M., Cartwright, J.A., Foschi, M., Shipp, R.C., & Van Rensbergen, P., 2016. Structure II gas hydrates found below the bottom-simulating reflector. Geophys. Res. Lett., 43, 5696–5706. https://doi.org/10.1002/2016GL069452.

Paganoni, M., Cartwright, J.A., Foschi, M., Shipp, G.R., & Van Rensbergen, P., 2018. Relationship between fluid-escape pipes and hydrate distribution in offshore Sabah (NW Borneo). Marine Geology, 395, 82–103. http://dx.doi.org/10.1016/j.margeo.2017.09.010.

Pecher, I.A., & Henrys, S.A., 2003. Potential gas reserves in gas hydrate sweet spots on the Hikurangi Margin, New Zealand. Institute of Geological and Nuclear Sciences, 2003/23.

Reagan, M.T., & Moridis, G.T., 2007. Oceanic gas hydrate instability and dissociation under climate change scenarios. Geophys. Res. Lett., 34, L22709. https://doi.org/10.1029/ 2007GL031671.

Riedel, M., Collett, T.S., Malone, M.J., and the IODP Expedition 311 Scientists, 2006. Stages of gas-hydrate evolution on the Northern Cascadia Margin. Sci. Dril., 3, 18–24. https://doi.org/10.2204/iodp.sd.3.04.2006.

Rose, P.R., 2001. Risk analysis and management of petroleum exploration ventures. AAPG Methods in Exploration, 12. https://doi.org/10.1306/Mth12792.

Ruppel, C.D., 2011. Methane hydrates and contemporary climate change. Nature Education Knowledge, 3(10): 29.

Ruppel, C.D., 2018. Gas hydrate in nature. U.S. Geological Survey, Fact Sheet 2017–3080, 4 p. https://doi.org/10.3133/fs20173080.

Ryan, W.B.F., Carbotte, S.M., Coplan, J.O., O'Hara, S., Melkonian, A., Arko, R., Weissel, R.A., Ferrini, V., Goodwillie, A., Nitsche, F., Bonczkowski, J., & Zemsky, R., 2009. Global multi-resolution topography synthesis. Geochem. Geophys. Geosyst., 10, Q03014. http://dx.doi.org/10.1029/2008GC002332.

Shepherd, M., 2009. Factors influencing recovery from oil and gas fields. In: Shepherd, M. (Ed.), Oil field production geology, AAPG Memoir, 91, 37-46.

Sloan, E.D. Jr., 1998. Clathrate hydrates of natural gases (Second Edition). Marcel Dekker Inc., New York, Basel. 705 p.

Su, M., Yang, R., Wang, H., Sha, Z., Liang, J., Wu, N., Qiao, S., & Cong, X., 2016. Gas hydrates distribution in the Shenhu area, northern South China Sea: Comparisons between the eight drilling sites with gas-hydrate petroleum system. Geologica Acta, 14(2), 79-100. https://doi.org/10.1344/GeologicaActa2016.14.2.1.

Su, P., Lin, L., Lv, Y., Liang, J., Sun, Y., Zhang,W., He, H., Yan, B., Ji, Z., & Wang, L., *et al*., 2022. Potential and distribution of natural gas hydrate resources in the South China Sea. J. Mar. Sci. Eng., 10, 1364. https://doi.org/10.3390/jmse10101364.

Torres, M.E., Tréhu, A.M., Cespedes, N., Kastner, M., Wortmann, U.G., Kim, J.-H., Long, P., Malinverno, A., Pohlman, J.W., Riedel, M., & Collett, T., 2008. Methane hydrate formation in turbidite sediments of northern Cascadia, IODP Expedition 311. Earth and Planetary Science Letters, 271, 170–180.

Tréhu, A.M., Bohrmann, G., Rack, F.R., Torres, M.E., and the Leg 204 Scientific Party, 2003. ODP Leg 204: Gas hydrate distribution and dynamics beneath Southern Hydrate Ridge. JOIDES Journal, 29(2), 6-8.

Tréhu, A.M., Long, P.E., Torres, M.E., and the Leg 204 Scientific Party, 2004. Three-dimensional distribution of gas hydrate beneath southern Hydrate Ridge: Constraints from ODP Leg 204. Earth and Planetary Science Letters, 222, 845 – 862.

Vijayan, V.R., Stagg, H., & Foss, C., 2013. Crustal character and thickness over the Dangerous Grounds and beneath the Northwest Borneo Trough. Journal of Asian Earth Sciences, 76, 389-398. http://dx.doi.org/10.1016/j.jseaes.2013.06.004.

Waite, W.F., Ruppel, C.D., Boze, L.-G., Lorenson, T.D., Buczkowski, B.J., McMullen, K.Y., & Kvenvolden, K.A., 2020. Preliminary global database of known and inferred gas hydrate locations. U.S. Geological Survey data release. https://doi.org/10.5066/P9llFVJM.

Wang, J., & Lau, H.C., 2020. Thickness of gas hydrate stability zone in permafrost and marine gas hydrate deposits: Analysis and implications. Fuel, 282, 118784. https://doi.org/10.1016/j.fuel.2020.118784.

Wang, S., Yan, W., & Song, H., 2006. Mapping the thickness of the gas hydrate stability zone in the South China Sea. Terr. Atmos. Ocean. Sci., 17(4), 815-828.

Wang, X., Hutchinson, D.R., Wu, S., Yang, S., & Guo, Y., 2011. Elevated gas hydrate saturation within silt and silty clay sediments in the Shenhu area, South China Sea. Journal of Geophysical Research, 116, B05102. https://doi.org/10.1029/2010jb007944.

Wang, X., Zhou, J., Li, L., Jin, J., Li, J., Guo, Y., Wang, B., Sun, L., & Qian, J., 2022. Bottom simulating reflections in the South China Sea. In: Mienert, J., Christian Berndt, Anne M. Tréhu, Angelo Camerlenghi, & Char-Shine Liu (Eds.), World atlas of submarine gas hydrates in continental margins. Springer, Cham, Switzerland. 514 p. https://doi.org/10.1007/978-3-

030-81186-0_13.

Warren, J.K., Cheung, A., & Cartwright, J.A., 2010. Organic geochemical, isotopic, and seismic indicators of fluid flow in pressurized growth anticlines and mud volcanoes in modern deep-water slope and rise sediments of offshore Brunei Darussalam: Implications for hydrocarbon exploration in other mud- and salt-diapir provinces. In: Wood, L. (Ed.), Shale tectonics. AAPG Memoir, 93, 163-196.

Wu, J., McClay, K., & de Vera, J., 2020, Growth of triangle zone fold-thrusts within the NW Borneo deep-water fold belt, offshore Sabah, southern South China Sea. Geosphere, 16(1), 329–356. https://doi.org/10.1130/GES02106.1.

Yamamoto, K., 2022. Gas hydrate drilling in the Nankai Trough, Japan. In: Mienert, J., Christian Berndt, Anne M. Tréhu, Angelo Camerlenghi, & Char-Shine Liu (Eds.), World atlas of submarine gas hydrates in continental margins. Springer, Cham, Switzerland. 514 p. https://doi.org/10.1007/978-3-030-81186-0_15.

Yamamoto, K., Wang, X.-X., Tamaki, M., & Suzuki, K., 2019. The second offshore production of methane hydrate in the Nankai Trough and gas production behavior from a heterogeneous methane hydrate reservoir. RSC Adv., 9, 25987–26013. https://doi.org/ 10.1039/c9ra00755e.

Ye, J.-L., Qin, X., Xie, W., and 25 others, 2020. The second natural gas hydrate production test in the South China Sea. China Geology, 2, 197-209. https://doi.org/10.31035/cg2020043.

Yu, T., Guan, G., Abudula, A., Yoshida, A., Wang, D., & Song, Y., 2019. Enhanced gas recovery from methane hydrate reservoir in the Nankai Trough, Japan. Energy Procedia, 158, 5213–5218.

Zhang, R.-W., Lu, J., Wen, P., Kuang, Z., Zhang, B., Xue, H., Xu, Y., & Chen, X., 2018. Distribution of gas hydrate reservoir in the first production test region of the Shenhu area, South China Sea. China Geology, 4, 493−504. https://doi.org/10.31035/cg2018049.

Zhang, X., Hu, T., Pang, X.-Q., Hu, Y., Wang, T., Wang, E.-Z., Xu, Z., Liu, X.-H., & Wu, Z.-Y., 2021. Evaluation of natural gas hydrate resources in the South China Sea by combining volumetric and trend-analysis methods. Petroleum Science, 19(1), 37-47. https://doi.org/10.1016/j.petsci.2021.12.008.

Manuscript received 13 February 2022;
Received in revised form 25 March 2022;
Accepted 28 March 2022
Available online 30 November 2022